scientific reports

Check for updates

OPEN

Improving damping capabilities in low-rise frames using reinforced rubberized concrete: A comprehensive study

Ahed Habib[1], Moussa Leblouba[2], M. Talha Junaid[2], Salah Altoubat[2], Mohamed Maalej[2] & Maan Habib[3]✉

Over the past decade, extensive research has been conducted to investigate the properties and behavior of rubberized concrete as a sustainable green alternative to conventional concrete. This research involves replacing natural aggregates with rubber particles from discarded tires. Generally, these studies have shown an enhancement in ductility, energy dissipation, and the damping ratio of rubberized concrete. However, a significant reduction in mechanical properties, such as compressive and tensile strength, and modulus of elasticity, has been noted compared to standard concrete. Currently, the literature lacks a comprehensive numerical study that could provide structural engineers with a complete understanding of the seismic performance of rubberized concrete frames. Consequently, this study examines three low-rise RC frames subjected to sixty recorded ground motions (near-fault, pulse-like, and far-fault) using nonlinear response-history analysis, comparing rubberized concrete (RBC) with a control concrete (NC-C) and a similar-strength mix (NC-S). Across records, RBC exhibits lower base shear (mean reductions up to 11.6–13.8% versus NC-C and about 3–6% versus NC-S, depending on motion class), higher viscous damping energy (increases of 29–53%), and lower hysteretic energy (reductions of about 10–29%), while interstory drift ratios increase yet remain within ASCE 7 drift limits. Absolute floor accelerations reduce modestly (up to 11.8% in far-fault motions). The results indicate that substituting RBC can enhance damping efficiency and reduce seismic forces relative to both NC-C and NC-S under severe earthquakes at a drift trade-off.

Keywords Rubberized concrete, Structural material, Damping, Energy dissipation, Nonlinear response history analysis

Abbreviations

RBC	Rubberized Concrete
NC	Normal Concrete
NC-C	Normal Concrete (Control mix)
NC-S	Normal Concrete (Similar-strength mix)
RC	Reinforced Concrete
NRHA	Nonlinear Response-History Analysis
FEM	Finite Element Modeling
SSI	Soil–Structure Interaction
MCER	Maximum Considered Earthquake
ASCE	American Society of Civil Engineers
ACI	American Concrete Institute
NIST	National Institute of Standards and Technology
ATC	Applied Technology Council
FEMA	Federal Emergency Management Agency
PEER	Pacific Earthquake Engineering Research Center
MSE	Mean Square Error

[1]Research Institute of Sciences and Engineering, University of Sharjah, Sharjah, United Arab Emirates. [2]Department of Civil and Environmental Engineering, University of Sharjah, Sharjah, United Arab Emirates. [3]Faculty of Civil Engineering, Damascus University, Damascus, Syria. ✉email: maan.habib@gmail.com

PGA	Peak Ground Acceleration
PGV	Peak Ground Velocity
IDR	Interstory Drift Ratio
Vs30	Time-averaged shear-wave velocity in top 30 m(m/s)
SMS	MCER short-period spectral acceleration parameter(g)
SM1	MCER 1-s spectral acceleration parameter(g)
Tp	Pulse period (for pulse-like records)(s)
P–Δ	Second-order (geometric) effects(-)

Annually, a large number of moment-resisting frame buildings are constructed worldwide[1–7]. These structures' reinforced concrete (RC) elements are likely to sustain serious damage under moderate to strong ground motions, due to an energy-dissipation mechanism comprising rebar yielding, rebar slip, concrete cracking, and concrete spalling[8–11]. It is currently understood that incorporating a seismic control system into a framed structure can enhance its lateral performance by mitigating drift and inelastic deformations[12,13]. However, in developing countries situated in earthquake-prone zones, the financial burden arising from the design and implementation costs remains a significant challenge[14–16]. Therefore, an alternative low-cost solution is crucial to alleviate the impact of moderate earthquakes and to safeguard human lives against such disasters.

Recent studies have focused on using recycled rubber particles in concrete as an aggregate replacement, leading to the development of 'rubberized concrete'[17–20]. Rubberized concrete (RBC), compared to normal concrete (NC), not only offers environmental benefits but also excels in energy dissipation due to the rubber's inherent properties, thereby positively affecting the structures' vibration behavior[21,22]. Previous research has indicated a notable decrease in RBC's mechanical properties, such as compressive and tensile strength and modulus of elasticity, compared to NC mixtures with the same constituents but without rubber aggregates[23–28]. This decline is primarily due to the substitution of higher-strength aggregates with ones of lower strength[21] and the weaker bond between rubber aggregates and cement paste compared to that with natural aggregates, leading to a quicker rupture of concrete[29]. Conversely, RBC exhibits enhanced ductility, energy dissipation, and damping ratio relative to NC mixtures[17,19,20,27,30]. Mendis et al.[31] observed that RBC demonstrates a strength development rate, splitting tensile strength, modulus of rupture, modulus of elasticity, and stress–strain behavior comparable to other mixtures of similar strength, irrespective of the rubber content. Youssf et al.[32] found that reinforced RBC columns could withstand similar lateral loads as reinforced NC columns, despite the former's compressive strength being 28% lower. Additionally, the backbone curves of both reinforced NC and RBC columns were nearly parallel, suggesting similar behavior under cyclic loading and indicating RBC's suitability for use in RC columns without detrimentally affecting their general hysteretic behavior[33]. Xue & Shinozuka[21] concluded from their shaking table tests that RBC usage in structures significantly reduces seismic demand due to increased damping ratio. Furthermore, Moustafa et al.[8] reported that in large-scale RC columns, RBC delayed rebar fracture significantly compared to conventional columns during shaking table tests. These findings suggest that the differences in energy dissipation and seismic demand between NC and RBC structures are mainly attributable to variations in material damping ratio and modulus of elasticity, respectively.

Thus, RBC represents a promising method for enhancing the seismic performance of RC structures by increasing structural damping energy and reducing seismic demand, similar to passive control systems, though the latter may offer superior performance at a considerably higher cost. This study aims to advance research in RBC and RC structures by proposing a method to improve vibration behavior and energy dissipation and to reduce the seismic demand of RC moment-resisting frames. This will be achieved through a computer-based numerical investigation using finite element models (FEMs), analyzed via the nonlinear response history analysis method (NRHA). The study will examine the behavior of three low-rise RC moment-resisting frames under sixty different real ground motion records. Subsequently, the outputs of the nonlinear time history analysis will serve as inputs for a detailed statistical investigation, providing crucial insights into RBC's contribution to the seismic behavior of reinforced concrete frames. This knowledge, currently absent from the literature, is vital for verifying the reliability of such materials in construction, especially in earthquake-prone regions.

Materials and methods

Selected structures

In order to seismically investigate the performance of rubberized concrete, a three-story RC moment-resisting frame, as shown in Fig. 1, was selected. This frame represents a typical low-rise building designed in the late 1990 s in the Middle East. Similar to the study by Kitayama & Constantinou[12], it is assumed that the building is located in a site class D, with the MCE_R response spectrum described by parameters $S_{MS} = 1.875$ g and $S_{M1} = 0.9$ g.

Material properties

Habib et al.[27] noted that coarse rubber particles in concrete yield better energy dissipation and damping ratios than finer particles. The properties of both NC and RBC, used in this study, were derived from research by Xue & Shinozuka[21], where 15% of coarse aggregates were replaced by 6 mm recycled tire rubber. The RBC mixture's properties, presented in Table 1, show that adding rubber particles reduced the compressive strength by approximately 43.5% and the modulus of elasticity by 36.8%, compared to control concrete (NC-C). Conversely, the damping ratio of a reinforced concrete column made from RBC showed a 69% increase, while its natural frequency decreased by 28%. These variations are likely to significantly alter the seismic behavior of RC structures in terms of seismic demand and energy distribution.

In order to control the influence of RBC, a C20/25 conventional concrete was chosen for comparison with RBC and a similar strength concrete (NC-S). The properties of this concrete, defined according to Eurocode 2, are detailed in Table 1.

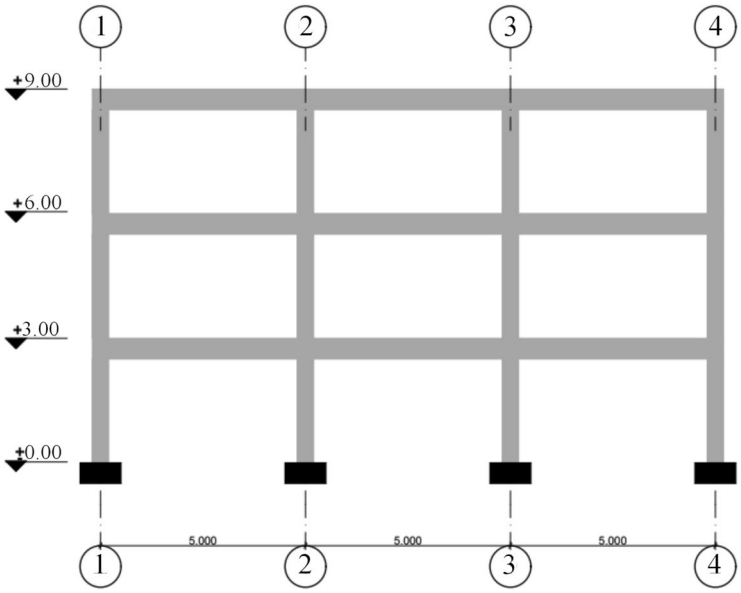

Fig. 1. Selected frame structure (in meters).

	RBC	NC-S	NC-C
Compressive strength (MPa)	21.5	20	38
Modulus of elasticity (GPa)	21	30	33.2
Density of concrete (kg/m^3)	2171	2549	2475
Column damping ratio (%)	8.1	-	4.8
Column natural frequency (Hz)	5.65	-	7.85

Table 1. Properties of normal and rubberized concrete used for jacketing.

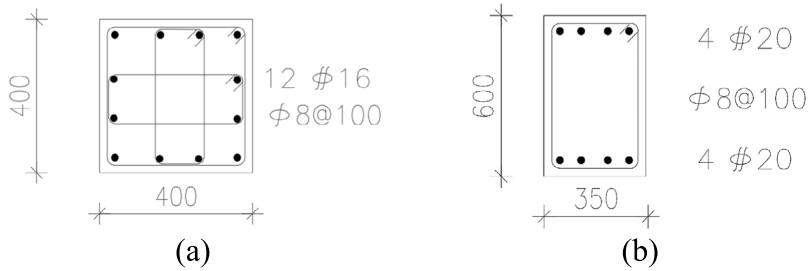

Fig. 2. Dimensions and reinforcements of the structural elements (**a**) column, and (**b**) beam (in millimeters).

Preliminary design of the structure

The preliminary design of the selected structures involved creating a 2D numerical model in SAP 2000. The stiffness properties of beam and column sections for linear elastic analysis were defined, considering the influence of cracked sections, using the effective stiffnesses from ACI 318[34]. The design incorporated both gravity loads from the building and seismic loads applied using the equivalent lateral force method from ASCE 7[35]. The frame's structural elements were designed to sustain moderate damage, resulting in relatively high interstory drift ratios under earthquake excitations. This design enables the investigation of the structures' energy dissipation. Beam and column sections, along with their reinforcement configurations, are illustrated in Fig. 2.

Nonlinear modeling

Nonlinear modeling followed the NIST GCR 17–917-46v3 guidelines[36]. Fiber-section hinges were implemented using unconfined compressive stress–strain behaviors of NC and RBC based on data in Table 1. Confined material models, as shown in Fig. 3, were developed from these relations and the reinforcement configurations using a method proposed by Mander et al.[37]. Stress–strain behaviors of steel reinforcements followed Park & Paulay's model, as depicted in Fig. 4[38]. Therefore, the fiber sections in this study adopt an unconfined concrete

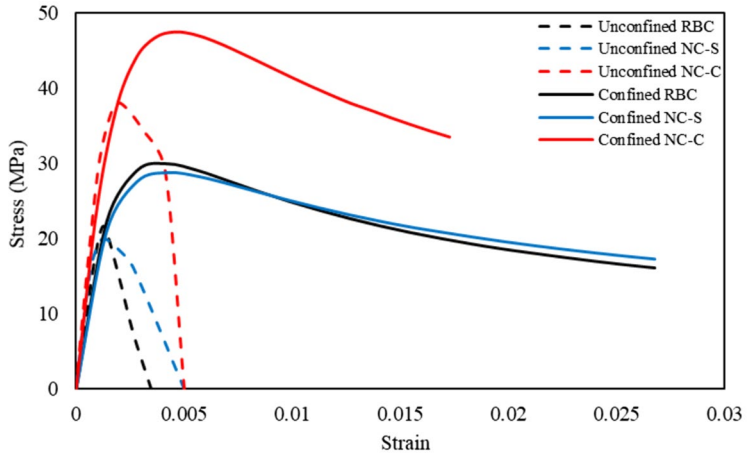

Fig. 3. Concrete stress–strain behavior.

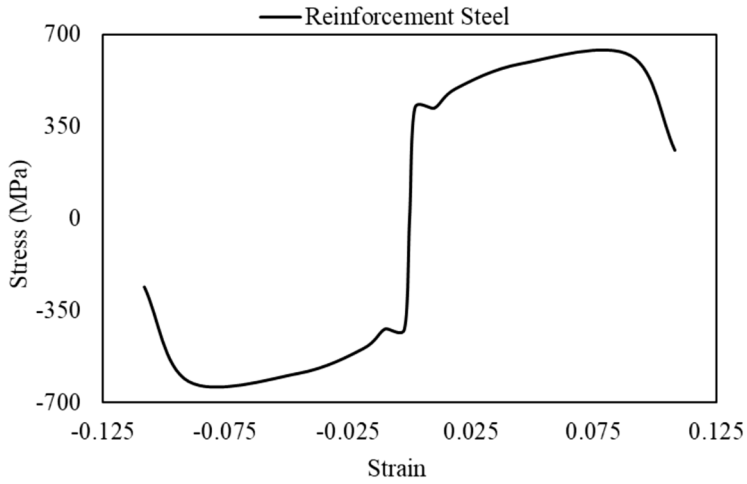

Fig. 4. Steel reinforcement stress–strain behavior.

envelope consistent with the measured compressive strengths/moduli in Table 1 and a confined core envelope computed with the Mander et al.[37] model. Although rubberization alters post-peak softening, the Mander formulation governs the confinement effect provided by transverse reinforcement and remains appropriate for the core stress–strain envelope when the unconfined backbone reflects the measured RBC properties. Tension cracking and softening are represented implicitly by the fiber discretization using the unconfined envelope in the cover; no explicit bond-slip springs are introduced at bar locations. This modeling choice follows prior frame-level studies where the focus is on system-level energy partitioning rather than bar anchorage mechanics; its implication is discussed as a limitation in the conclusions.

It is anticipated that RC members will exhibit behavior beyond their cracked state during catastrophic events[39]. To model a realistic analysis, the lateral stiffness of structural elements was characterized in terms of effective rigidity, calculated using mathematical expressions proposed by Kwon[40]. This calculation considers deformations from flexure, bar-slip, and shear.

The nonlinear behavior of structural elements was simulated using the fiber hinge model. Following Kalantari and Roohbakhsh[41], beams and column sections were divided into three fiber parts: the cover, built using the unconfined concrete model; the core, built using the confined concrete model; and steel reinforcement fibers.

In order to represent the inherent damping in a conventional concrete structure, Rayleigh damping was employed in the nonlinear direct integration analysis. Alpha and beta coefficients were calculated to yield a 2.5% damping ratio at 1.5 and 0.25 times the first fundamental mode period for the NC-S and NC-C models. Given the increased damping capability of rubberized concrete, the damping ratio for the RBC model was set at 1.69 times that of the NC-C model, resulting in a 4.225% ratio at the same periods, in line with Xue & Shinozuka's[21] findings.

Lastly, the beam-column panel zones were modeled without explicitly simulating joint stiffness. Instead, line elements extending from the beams and columns into the panel zone were used, as discussed in NIST GCR 17–917-46v3[36]. This choice follows recommended practice for building-level NRHAs where the objective

is to compare material scenarios under identical modeling assumptions. Joint shear deformation does dissipate energy; however, because all three frames share the same joint idealization, the relative findings, higher viscous damping energy and lower hysteretic energy for RBC, and reduced base shear, remain unaffected in direction. The omission of explicit joint shear is noted as a limitation in this study. P-delta effects were considered in the analysis, while soil-structure interactions were omitted by fixing the lower node of each column, preventing rotation and displacement at the frame's base. The fixed-base idealization is justified for the selected low-rise frames on Site Class D because the expected foundation compliance produces period lengthening and damping changes smaller than the material-induced differences studied here; moreover, applying the same base idealization to all mixes preserves the validity of the pairwise comparisons.

Ground motion records

Sixty real ground-motion records, obtained from the Pacific Earthquake Engineering Research Center (PEER), were selected for this study. These records are categorized into near-fault, pulse-like, and far-fault types. The selection, presented in Table 2, was based on criteria such as the record's magnitude, shear wave velocities of the soil profile, distance to the fault, and the ratio of peak ground acceleration (PGA) to peak ground velocity (PGV), which is discussed in detail in Sect. Influence of Ground Motion Intensity on the Performance of RBC.

Michaud and Léger[42] compared various earthquake scaling methods, including those recommended by ACT[43] and ASCE 7[44], and the mean square error (MSE) minimizing approach. They concluded that the MSE scaling approach yields superior results compared to the ACT[43] and ASCE 7[44] techniques. Consequently, this study adopted the MSE scaling method to scale the records for periods between 0 and 5 s to the targeted spectrum, as illustrated in Fig. 5. This process involved calculating a single scale factor for each record and then applying a modification parameter to these factors to minimize the MSE value. This modification ensures the mean spectrum of the final scaled ground motions closely matches the target spectrum over the desired period range. Each earthquake record was further enhanced by adding 15 s of trailing zeros at the end to represent the structure's free vibration response post-excitation[12].

Therefore, in this study, each record was baseline-corrected and band-pass filtered within the usable frequency range provided by PEER metadata; units were maintained as recorded and converted consistently within SAP2000. A single horizontal component per station was used (the component with the larger PGA when both were available); vertical components were not considered because the study targets lateral energy partitioning in low-rise frames. Mean-square-error scaling was applied over $T \in [0,5]$ s using a single scale factor per record updated by the MSE-minimizing modifier. No record was excluded for excessive amplification under this criterion. Appending 15 s of trailing zeros allows the structures to undergo free vibration, enabling unambiguous computation of damping energy without altering the strong-motion content; the energy balance was verified to stabilize during this tail, consistent with Kitayama & Constantinou[12].

Model validation

As previously discussed, the difference between a Rubberized Bitumen Composite (RBC) structure and a Normal Concrete Composite (NC-C) lies in their dynamic behavior, not in mechanical performance. RBC concrete exhibits mechanical performance similar to that of conventional concrete with comparable mechanical properties. Therefore, the nonlinear hysteretic behaviors of RBC members will mirror those of NC, while factors like vibration performance, damping energy, and seismic demand will vary based on the material's damping ratio and modulus of elasticity, and the resulting structural first mode frequency. Similar to Mir & Rai[45], this study's procedure for assessing the accuracy and validity of the numerical models focused on the first mode frequencies. The study compared the ratios of RBC frequency to NC-C frequency between the full frame models used here and the experimental study on single RC columns by Xue & Shinozuka[21], as demonstrated in Table 3.

Furthermore, to validate the numerical model's capability in capturing RBC's nonlinear behavior, the same earthquake record used in Xue & Shinozuka's[21] shaking table test was applied to the numerical model. Appropriate scaling was employed to achieve a similar damage level as reported in the reference study. Nonlinear response history analysis was conducted to obtain the peak acceleration responses, and the variations are reported in Table 4. The error reported in Tables 3–4 is the relative deviation of the numerical RBC-to-NC-C response ratio from the corresponding experimental ratio,

$$\text{Error}(\%) = \frac{\mid (R_{\text{num}}/C_{\text{num}}) - (R_{\text{exp}}/C_{\text{exp}}) \mid}{(R_{\text{exp}}/C_{\text{exp}})} \times 100 \tag{1}$$

where R and C denote RBC and NC-C responses, respectively.

For the acceleration case, peak values under the same input (as reported by Xue & Shinozuka[15]) were used. The original tests did not publish synchronized displacement or energy time histories for the same inputs; therefore, RMS time-history errors or hysteresis overlays could not be reproduced. On the other hand, this study validates the modal-property ratios and the peak response ratios at the element level, then confirms that the direction of change (lower frequency, higher effective damping, reduced peak acceleration) persists in full-frame NRHAs. This is appropriate because all conclusions are drawn from paired, relative comparisons (RBC vs NC-S/NC-C) over 60 recorded motions.

In general, the comparison between experimental measurements and the results from the finite element models using SAP2000[46] reveals only minor variations. These discrepancies are attributed to factors like the consideration of beam-column joints and the scale of the RC column in Xue & Shinozuka's[21] experimental study, versus the behavior of a full frame. Hence, the error in these ratios provides a reasonable estimate of accuracy.

Group	RSN	Year	Earthquake Name	Tp (s)	Magnitude (Mw)	Vs30 (m/s)	Duration (s)	Fault Distance (km)	PGA (g)	PGV (m/s)
Near-Fault	126	1976	Gazli, USSR	-	6.8	259.59	14	5.46	0.702	0.662
	160	1979	Imperial Valley-06	-	6.53	223.03	38	2.66	0.599	0.468
	165	1979	Imperial Valley-06	-	6.53	242.05	52	7.29	0.270	0.248
	269	1980	Victoria, Mexico	-	6.33	242.05	19	7.27	0.045	0.063
	368	1983	Coalinga-01	-	6.36	257.38	58	8.41	0.602	0.605
	564	1986	Kalamata, Greece-01	-	6.2	382.21	30	6.45	0.239	0.335
	779	1989	Loma Prieta	-	6.93	594.83	25	3.88	0.570	0.961
	821	1992	Erzican, Turkey	-	6.69	352.05	21	4.38	0.496	0.782
	825	1992	Cape Mendocino	-	7.01	567.78	30	6.96	1.494	1.223
	949	1994	Northridge-01	-	6.69	297.71	40	8.66	0.345	0.411
	1490	1999	Chi-Chi, Taiwan	-	7.62	542.41	90	9.49	0.146	0.367
	1494	1999	Chi-Chi, Taiwan	-	7.62	460.69	90	5.28	0.146	0.460
	1605	1999	Duzce, Turkey	-	7.14	281.86	26	6.58	0.404	0.712
	1612	1999	Duzce, Turkey	-	7.14	551.3	41	4.17	0.137	0.103
	3943	2000	Tottori, Japan	-	6.61	616.55	300	9.12	0.274	0.153
	3979	2003	San Simeon, CA	-	6.52	362.42	81	7.25	0.179	0.128
	4071	2004	Parkfield-02, CA	-	6	397.57	65	2.57	0.184	0.261
	4084	2004	Parkfield-02, CA	-	6	269.55	46	2.68	0.238	0.331
	5619	2008	Iwate	-	6.9	279.36	258	8.44	0.219	0.171
	8064	2011	Christchurch, New Zealand	-	6.2	198	27	3.26	0.384	0.545
Pulse-Like	159	1979	Imperial Valley-06	2.338	6.53	242.05	29	0.65	0.287	0.349
	170	1979	Imperial Valley-06	4.417	6.53	192.05	40	7.31	0.212	0.384
	171	1979	Imperial Valley-06	3.423	6.53	264.57	40	0.07	0.317	0.729
	285	1980	Irpinia, Italy-01	1.7133	6.9	649.67	37	8.18	0.130	0.236
	723	1987	Superstition Hills-02	2.394	6.54	348.69	23	0.95	0.432	1.343
	802	1989	Loma Prieta	4.571	6.93	380.89	40	8.5	0.514	0.416
	828	1992	Cape Mendocino	2.996	7.01	422.17	36	8.18	0.591	0.493
	982	1994	Northridge-01	3.157	6.69	373.07	29	5.43	0.411	1.115
	983	1994	Northridge-01	3.535	6.69	525.79	29	5.43	0.571	0.761
	1013	1994	Northridge-01	1.617	6.69	628.99	27	5.92	0.426	0.748
	1119	1995	Kobe, Japan	1.806	6.9	312	41	0.27	0.697	0.684
	1182	1999	Chi-Chi, Taiwan	2.5704	7.62	438.19	150	9.76	0.359	0.423
	1193	1999	Chi-Chi, Taiwan	6.65	7.62	427.73	90	9.62	0.282	0.511
	4040	2003	Bam, Iran	2.023	6.6	487.4	67	1.7	0.808	1.241
	4097	2004	Parkfield-02, CA	0.854	6	648.09	21	2.99	0.211	0.259
	4113	2004	Parkfield-02, CA	1.134	6	372.26	21	2.85	0.153	0.239
	4228	2004	Niigata, Japan	1.799	6.63	375	180	8.93	0.599	0.581
	4458	1979	Montenegro, Yugo	1.974	7.1	318.74	48	5.76	0.293	0.436
	6897	2010	Darfield, New Zealand	7.826	7	295.74	138	8.46	0.257	0.394
	6906	2010	Darfield, New Zealand	6.23	7	344.02	107	1.22	0.765	1.161

Continued

Group	RSN	Year	Earthquake Name	Tp (s)	Magnitude (Mw)	Vs30 (m/s)	Duration (s)	Fault Distance (km)	PGA (g)	PGV (m/s)
Far-Fault	9	1942	Borrego	-	6.5	213.44	50	56.88	0.066	0.062
	15	1952	Kern County	-	7.36	385.43	55	38.89	0.159	0.152
	17	1952	Southern Calif	-	6	493.5	40	73.41	0.036	0.031
	36	1968	Borrego Mtn	-	6.63	213.44	80	45.66	0.133	0.267
	51	1971	San Fernando	-	6.61	280.56	71	55.2	0.027	0.060
	56	1971	San Fernando	-	6.61	235	40	61.79	0.071	0.047
	68	1971	San Fernando	-	6.61	316.46	80	22.77	0.225	0.217
	122	1976	Friuli, Italy-01	-	6.5	249.28	40	33.4	0.062	0.106
	138	1978	Tabas, Iran	-	7.35	324.57	35	28.79	0.106	0.133
	163	1979	Imperial Valley-06	-	6.53	205.78	40	24.6	0.129	0.156
	169	1979	Imperial Valley-06	-	6.53	242.05	100	22.03	0.236	0.263
	172	1979	Imperial Valley-06	-	6.53	237.33	40	21.68	0.141	0.161
	280	1980	Trinidad	-	7.2	311.75	20	76.26	0.062	0.075
	294	1980	Irpinia, Italy-01	-	6.9	496.46	32	53.16	0.047	0.059
	295	1980	Irpinia, Italy-02	-	6.2	476.62	32	29.86	0.018	0.031
	302	1980	Irpinia, Italy-02	-	6.2	574.88	47	22.69	0.100	0.150
	322	1983	Coalinga-01	-	6.36	274.73	65	24.02	0.225	0.262
	323	1983	Coalinga-01	-	6.36	359.03	60	55.77	0.044	0.044
	325	1983	Coalinga-01	-	6.36	522.74	65	42.92	0.0260	0.036
	349	1983	Coalinga-01	-	6.36	360.92	60	33.07	0.074	0.090

Table 2. Selected earthquake records for NRHA.

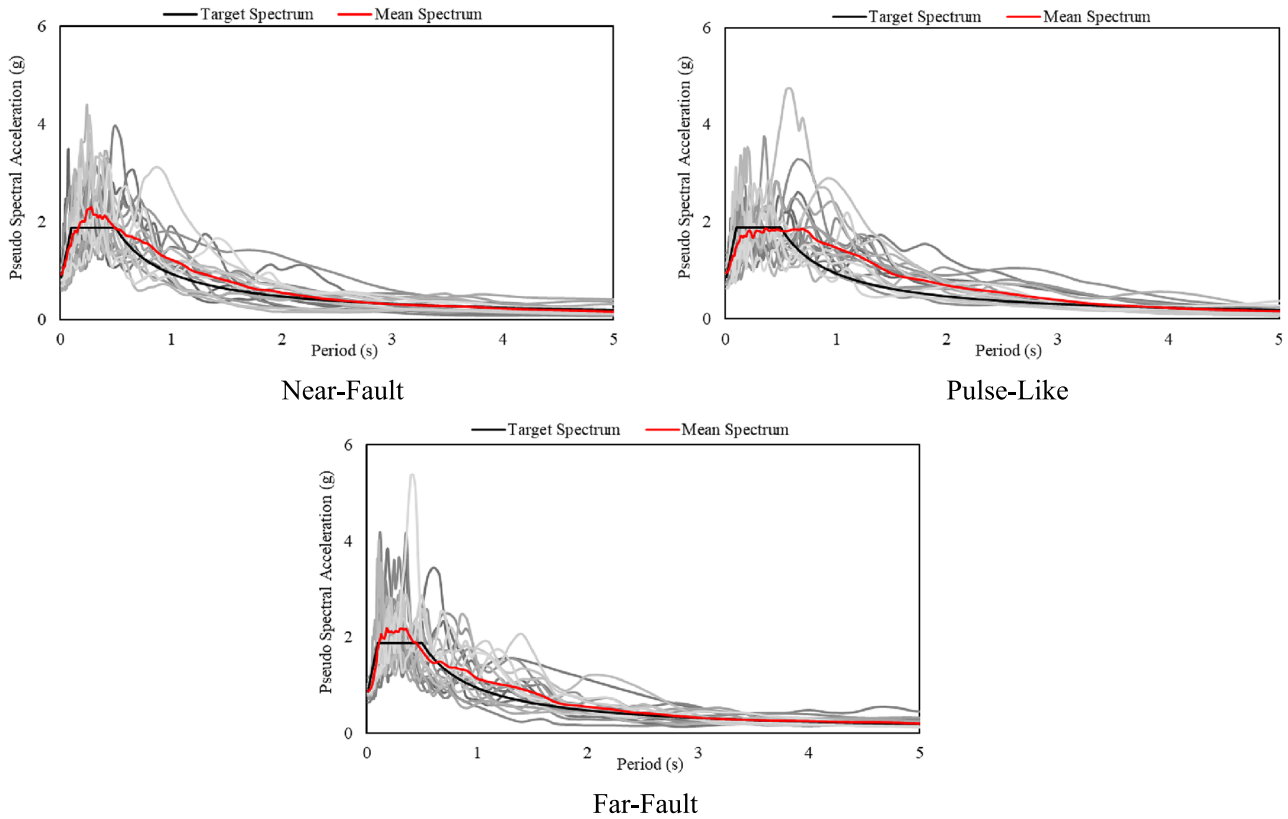

Fig. 5. Targeted spectrum versus the mean one for the selected earthquake groups.

	RBC (Hz)	NC-C (Hz)	$\frac{RBC}{NC-C}$	Error (%)
Reference RC columns by Xue & Shinozuka[21]	5.65	7.85	0.720	10.8
RC frames developed in this study	1.86	2.33	0.798	

Table 3. First mode frequencies of the experimental and numerical studies.

	RBC (m/s^2)	NC-C (m/s^2)	$\frac{RBC}{NC-C}$	Error (%)
Shaking table tests of the reference RC columns by Xue & Shinozuka[21]	18.64	13.73	0.737	11.67
Finite element analysis of the RC frames developed in this study	18.24	15.02	0.823	

Table 4. Peak acceleration responses of the experimental and numerical studies.

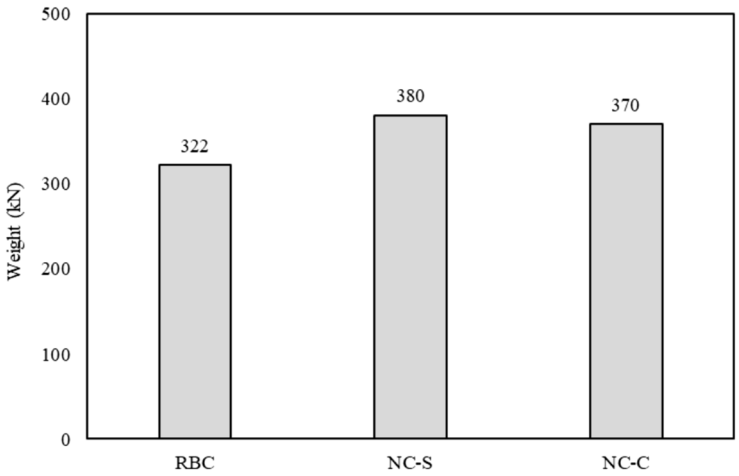

Fig. 6. Weight of the investigated frames.

Results

Seismic weight

In this study, the seismic weight was calculated as the full dead load on the frames and a 25% of the live load as highlighted in the ASCE 7 standard. The weight of the frames, depicted in Fig. 6, decreased as expected when RBC was used. Moreover, the weight of the structure reduced proportionally with the increase in rubber aggregates content in the mixture. Su et al.[47] attribute this reduction to the significant difference in specific gravity between rubber and natural aggregates. In this investigation, the frame weight decreased by 15.3% and 13% for NC-S and NC-C, respectively, compared to the RBC structure. Therefore, incorporating RBC in a structure can significantly affect the building's frequency and the corresponding base shear forces.

Period of the structure

As previously presented, the difference in natural periods between RBC and NC structures is primarily due to reductions in modulus of elasticity and unit weight. In this study, the period of the RBC model, as shown in Fig. 7, increased by 17% and 25.2% compared to the NC-S and NC-C, respectively. Similar observations were reported in earlier studies on RBC components[21,27]. Therefore, these results indicate that RBC effectively increases the structure's fundamental period compared to both NC-S and NC-C cases, consequently reducing its base shear forces in a manner akin to a base isolation system, albeit with less efficiency.

Story shear and overturning moment

Generally, NC frames exhibit higher story forces, as depicted in Fig. 8, and larger overturning moments, shown in Fig. 9, compared to the RBC model, regardless of the earthquake group applied. The results demonstrate a decrease of 3%, 3.12%, and 5.75% in the average base shear of RBC compared to NC-S, and a substantial reduction of 11.6%, 11.62%, and 13.8% compared to NC-C for near-fault, pulse-like, and far-fault earthquakes, respectively. These findings suggest that RBC reduces seismic forces compared to both NC-S and NC-C mixtures under earthquake excitations. Xue & Shinozuka[21] drew a similar conclusion in their component-level investigations.

While comparing mean story shear forces and mean overturning moments offers valuable insights into the effect of the significant increase in the period of RBC structures, it is crucial to examine the response to individual

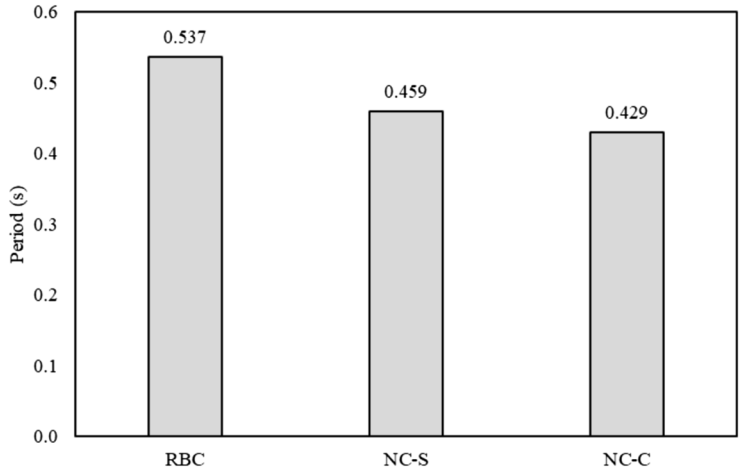

Fig. 7. Fundamental period of the investigated frames.

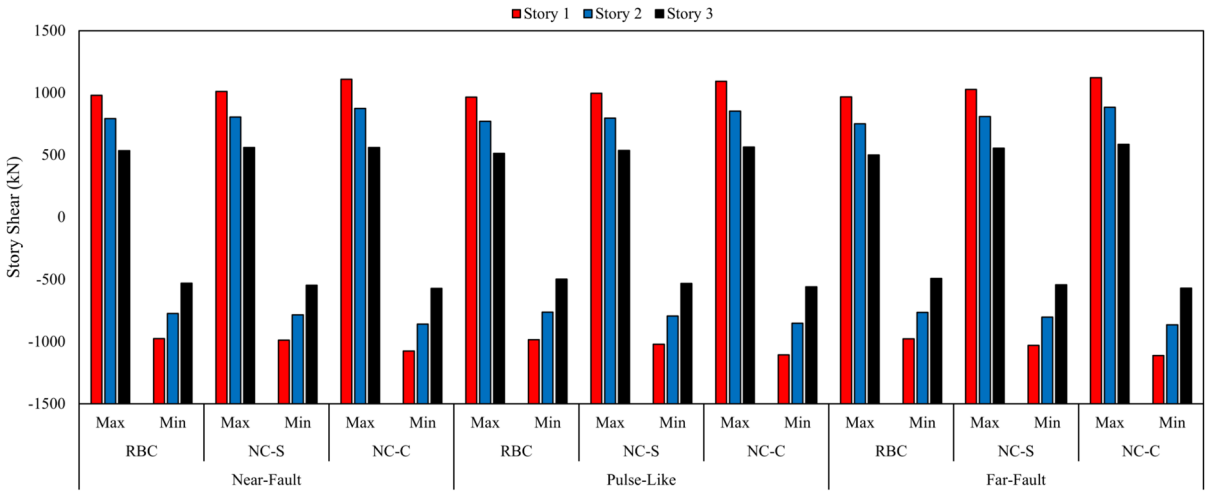

Fig. 8. Mean story shear of the investigated structures.

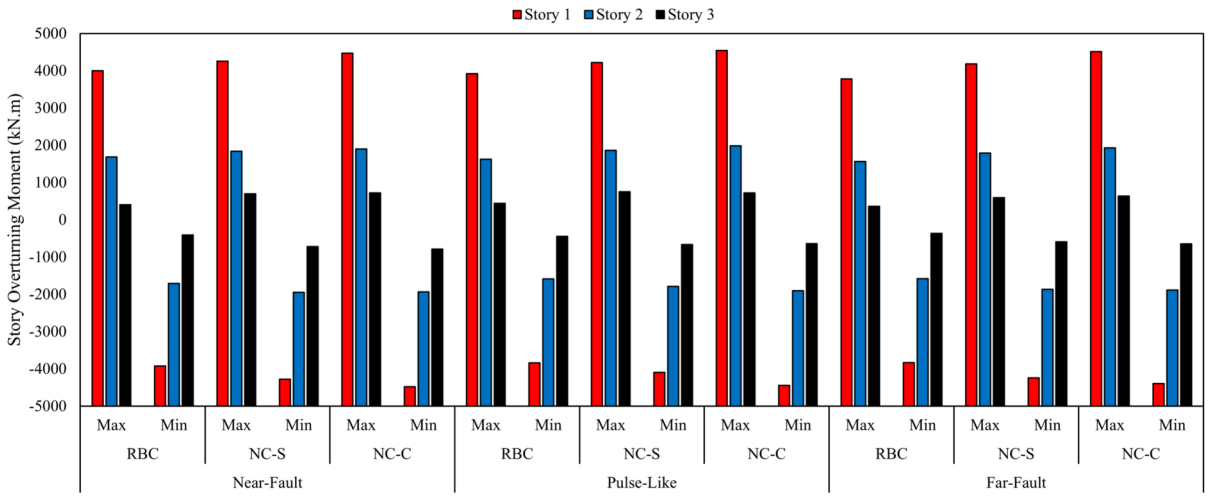

Fig. 9. Mean overturning moment of the investigated structures.

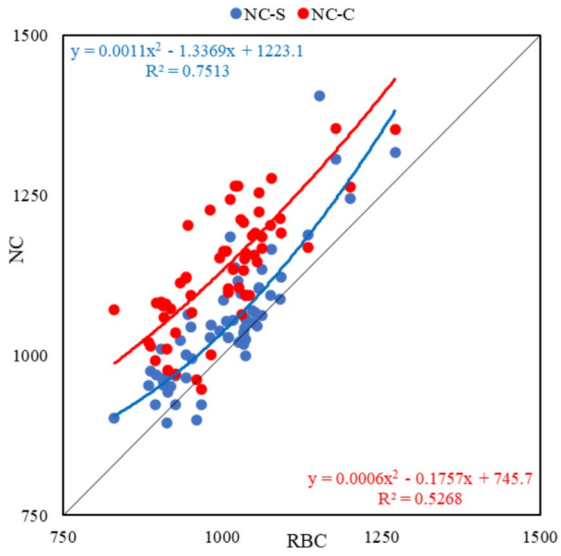

Fig. 10. Base shear (kN) of RBC versus NC.

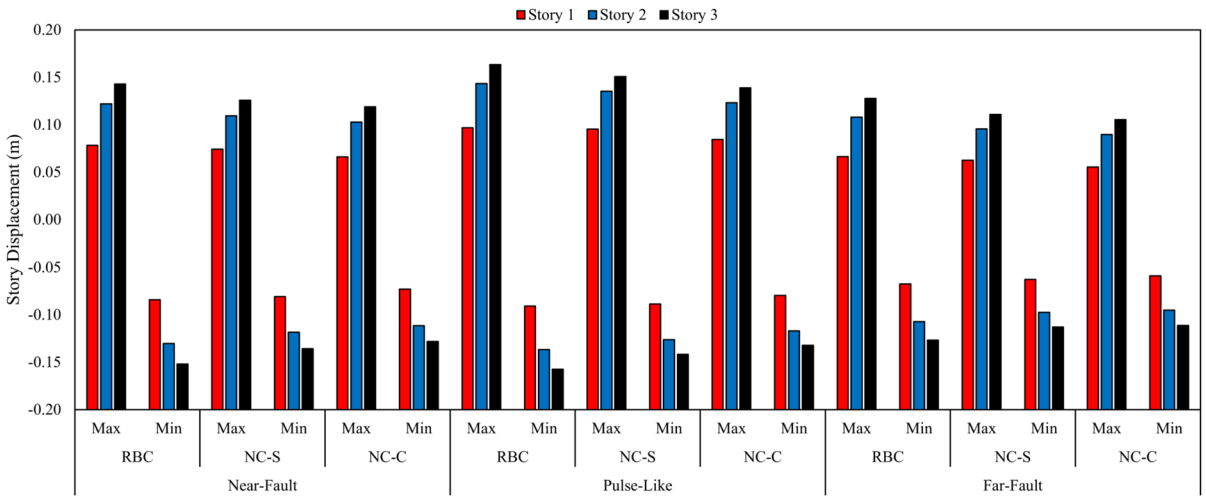

Fig. 11. Mean story displacement of the investigated structures.

earthquakes. This is because seismic forces largely depend on the spectrum shape of the ground motion records, meaning that RBC might have a higher seismic demand in certain earthquakes. In Fig. 10, a line of equality is drawn to represent points where X (RBC) and Y (NC) coordinates are equal. Thus, if a point lies above this line, it indicates that the Y coordinate (NC) is higher than the X coordinate (RBC). This figure shows that for almost all earthquakes, the base shear of NC-C is higher, and similarly, the seismic forces for NC-S are mostly greater than those of RBC. Additionally, the regression lines of these points indicate a considerable increase in forces for NC models compared to RBC. These observations provide solid evidence of RBC's efficiency relative to both a similar strength concrete (NC-S) and the control (NC-C).

Story displacement and interstory drift ratios

In fact, the story displacement, shown in Fig. 11, and interstory drift ratios, illustrated in Fig. 12, of the RBC frame were higher than those of NC-S and NC-C. This is attributed to the reduced stiffness of the RBC model. As observed in Fig. 11, the mean roof displacement of RBC increased by 13%, 11%, and 15% compared to NC-S, and by 20.2%, 19.1%, and 21% compared to NC-C for near-fault, pulse-like, and far-fault earthquakes, respectively. Although the peak mean interstory drift ratios for RBC under all earthquake groups were higher than those of NC, these ratios did not exceed the 4% limitations in ASCE 7[35]. Moustafa et al.[8] observed similar behavior in their shaking table tests, concluding that RBC can provide higher drift capacity while maintaining integrity by delaying rebar fracture due to its higher energy dissipation capability.

Despite the mean of RBC being 11% to 15% higher than NC-S, Fig. 13 indicates that the peak interstory drift ratio points for NC-S versus RBC are mainly scattered and fluctuating along the equality line, with their

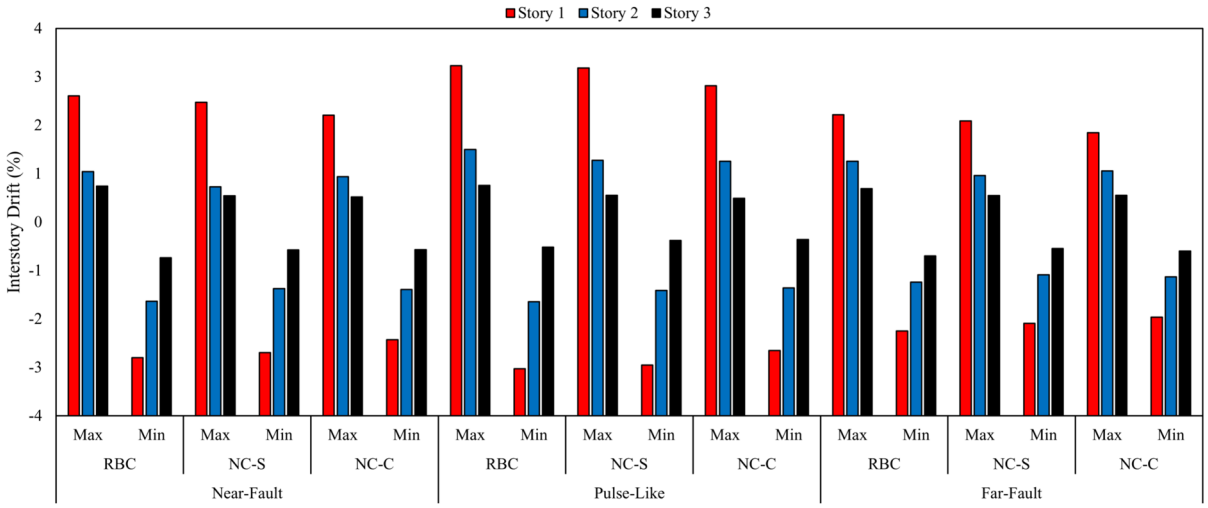

Fig. 12. Mean interstory drift ratio of the investigated structures.

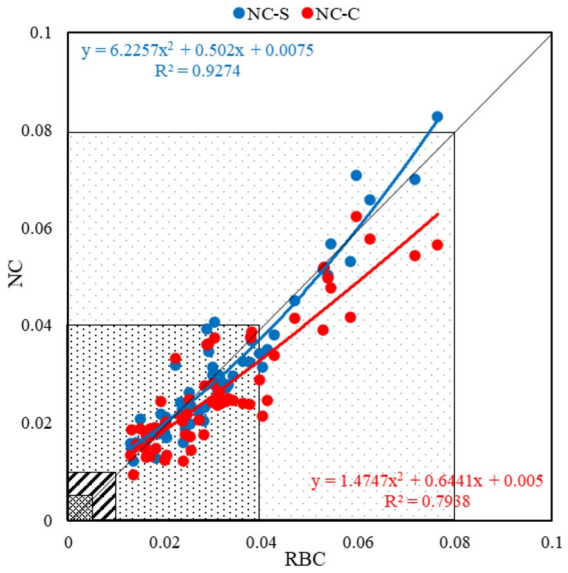

Fig. 13. Peak interstory drift ratio of RBC versus NC.

regression line generally lying over it. This suggests that in terms of interstory drift, both RBC and NC-S exhibit generally similar behavior, regardless of the difference in their periods of vibration, as also depicted in Fig. 12. Conversely, the behavior of the RBC frame is significantly higher than that of the NC-C frame in most cases, as seen in Fig. 13.

To confirm the design strategy of the weak frame used in this study, hatched squares in Fig. 13 represent four different damage limit states as defined by Hazus[48]. These limits are 0.5%, 1%, 3%, and 8% for slight, moderate, extensive, and complete collapse stages, respectively. Under the selected earthquakes, the frames primarily behaved within the extensive and complete damage states, adhering to the intended design pattern. However, NC-S typically exhibited higher drift values beyond the extensive limit state compared to RBC. Moreover, Fig. 13 reveals that the only case where a frame exceeded the complete damage state was in the NC-S model. This finding implies that, when comparing concretes of similar strengths, RBC slightly mitigates the maximum recorded drifts under severe ground motions that cause damage beyond the extensive limit state.

Floor accelerations

The mean absolute floor acceleration responses from the nonlinear time history analyses of each earthquake group are presented in Fig. 14. Generally, the acceleration responses of RBC closely match those obtained in the NC-S case. However, RBC consistently underperforms compared to NC-C, particularly excelling in far-fault excitations where it was 6.2% and 11.8% lower than NC-S and NC-C, respectively. This trend is further illustrated by the regression lines in Fig. 15, which suggest that RBC is more effective in reducing acceleration

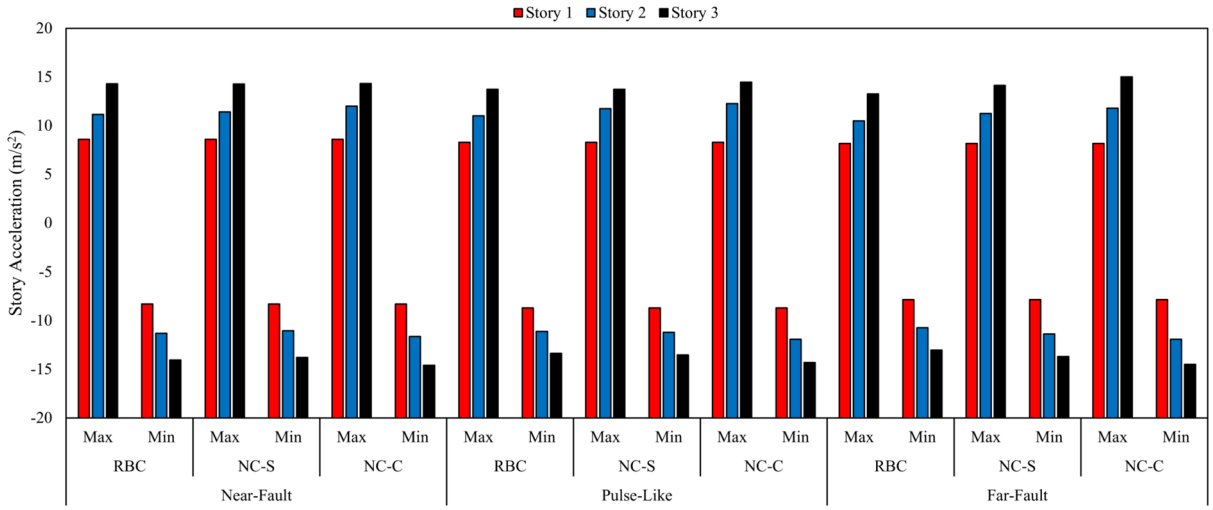

Fig. 14. Mean of the absolute floor accelerations of the investigated structures.

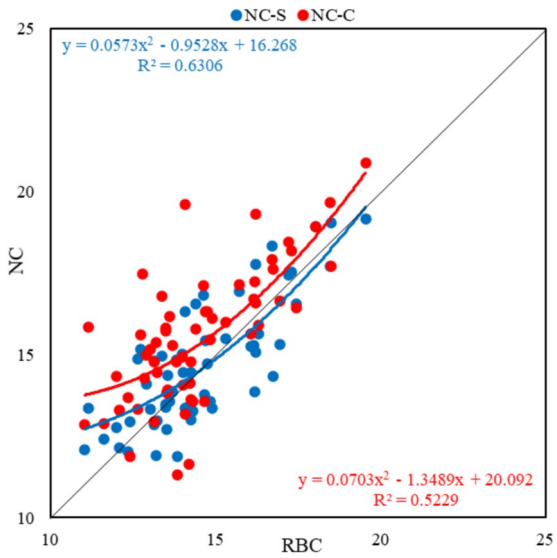

Fig. 15. Peak absolute roof accelerations (m/s^2) of RBC versus NC.

responses than NC. These findings indicate that using RBC likely results in less damage to the nonstructural elements of a building under maximum considered earthquake (MCER) ground motions compared to NC.

Energy dissipation

Figure 16 presents the results of input and nonlinear component energies in this study. As shown in Fig. 16-a, peak input energy values in the frames under investigation were consistent across different earthquake groups, a trend also reflected in Fig. 17-a, where the regression lines coincide with the equality line. Conversely, the RBC model demonstrated superior performance in damping energy, as evidenced by higher values in most earthquakes (Fig. 17-b) and increased means (Fig. 16-b) by 53.2%, 41%, and 39% compared to NC-S, and 42.5%, 31.3%, and 29% compared to NC-C for near-fault, pulse-like, and far-fault earthquakes, respectively. As Moustafa et al.[8] discussed, these outcomes are attributed to the viscoelastic nature of the rubber particles, enhancing the concrete's damping ratio. Hysteretic energy, which refers to energy dissipated through inelastic excursions during seismic excitation[49], shows that higher values indicate more plastic cracks and degradation in strength and stiffness. Although RBC's interstory drift ratios were generally higher than those of NC models, the peak hysteretic energies for both NC-S and NC-C (Fig. 17-c) were significantly higher than RBC. Moreover, the mean peak hysteretic energies (Fig. 16-c) increased by 18.5%, 16.5%, and 29.15% when comparing NC-S to RBC, and by 13.63%, 9.77%, and 19.35% for NC-C and RBC, respectively, in near-fault, pulse-like, and far-fault earthquakes. These findings align with Moustafa et al.[8] and suggest that RBC can mitigate damage in RC

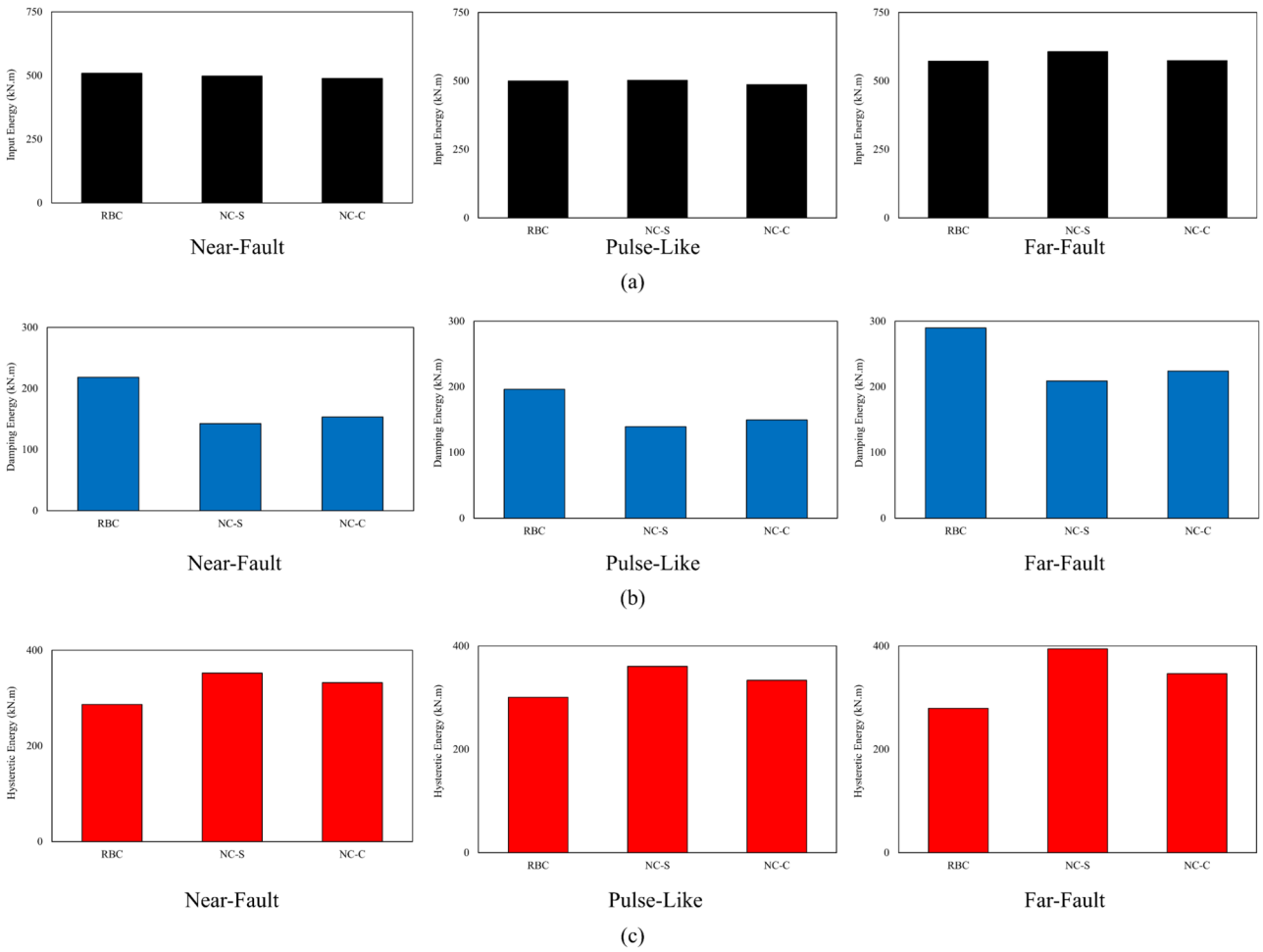

Fig. 16. Mean of the peak (**a**) input energy, (**b**) damping energy, and (**c**) hysteretic energy.

structures despite higher expected drifts. Thus, RBC positively influences the energy dissipation of RC frames compared to NC.

Influence of ground motion intensity on the performance of RBC

This section focuses on the impact of ground motion type and intensity on RBC's efficiency. Various earthquake intensity measurements, such as PGA, PGV, and the PGA/PGV ratio, are reported in the literature. Zhu et al.[50] proposed using the PGA/PGV ratio for ground motion characterization. Accordingly, three classes of PGA/PGV were defined, as shown in Table 5[51]. Generally, low PGA/PGV values significantly affect flexible structures with large periods, while high values critically impact stiff structures with shorter periods[52,53]. Consequently, earthquakes from all groups were selected, with a preference for those with medium PGA/PGV values to align with the properties of the investigated structure.

Two comparisons were made based on earthquake selection. The first compares the effects of ground motion groups, such as near-fault, pulse-like, and far-fault, each characterized by its PGA/PGV ratio. The second involves comparing three earthquakes from each PGA/PGV class for the aforementioned ground motion groups to thoroughly investigate the seismic behavior of frame structures in the time domain.

Figure 18 presents the first comparison. The general behavior observed in earlier parts of this study, lower base shear, higher damping energy, reduced hysteretic energy, increased interstory drift ratio, and decreased roof accelerations for RBC compared to NC-C, is evident in the box plot analyses of Fig. 18. Regarding the PGA/PGV influence on RBC's efficacy, higher base shear values are noted for PGA/PGV ratios between 0.5 and 1. Additionally, more significant reductions are observed in near-fault and pulse-like earthquakes compared to far-fault ones when contrasting RBC with NC-C, as shown in the box plots. However, the type or intensity of the earthquake did not significantly influence RBC's effects on damping energy. Moreover, the RBC's hysteretic energy reached its highest values in pulse-like earthquakes with a medium PGA/PGV ratio, whereas its most effective performance in reducing this energy component compared to NC-S and NC-C occurred in near-fault ground motions.

The maximum inter-story drift responses of the frames were observed in near-fault records. However, the most severe case for this parameter appears in pulse-like records, as they tend to cluster at higher values compared to the scattered behavior observed in near-fault cases and the lower responses in far-fault cases. Additionally,

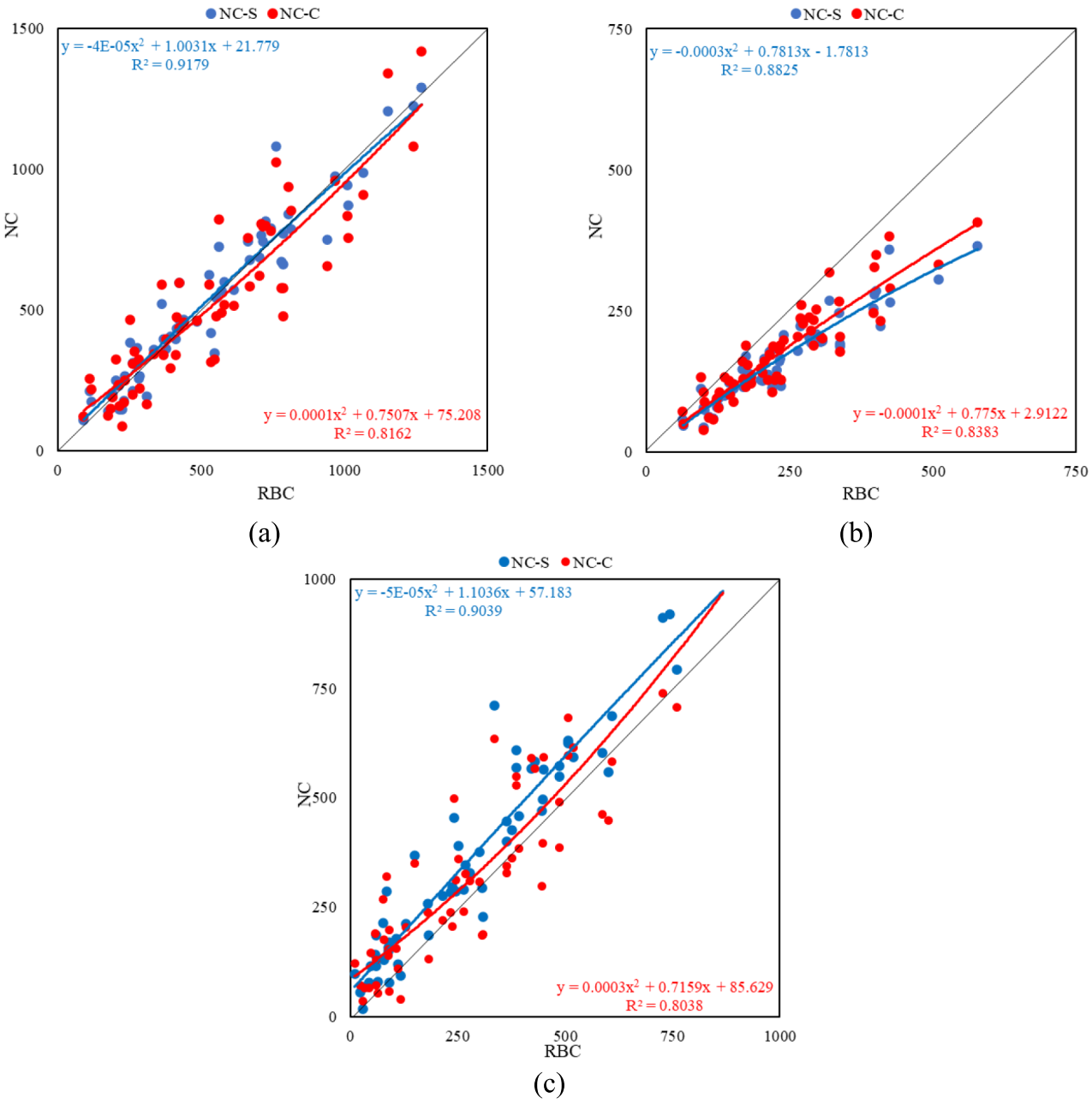

Fig. 17. Peak (**a**) input energy, (**b**) damping energy, and (**c**) hysteretic energy of RBC versus NC (in kN.m).

Class	Limits
Low	PGA/PGV < 0.8
Medium	0.8 ≤ PGA/PGV ≤ 1.2
High	1.2 < PGA/PGV

Table 5. Classifications of PGA/PGV ratios.

the intensity of ground motion significantly influences the response, with medium values producing the worst scenarios. Conversely, employing RBC yielded the best roof acceleration response during far-fault records, outperforming both NC-S and NC-C. Therefore, it can be inferred that the type and intensity of ground motions generally do not significantly influence the advantages of using RBC. These advantages include lower base shear, hysteretic energy, and roof accelerations, along with higher damping energy, as deduced from the box plots.

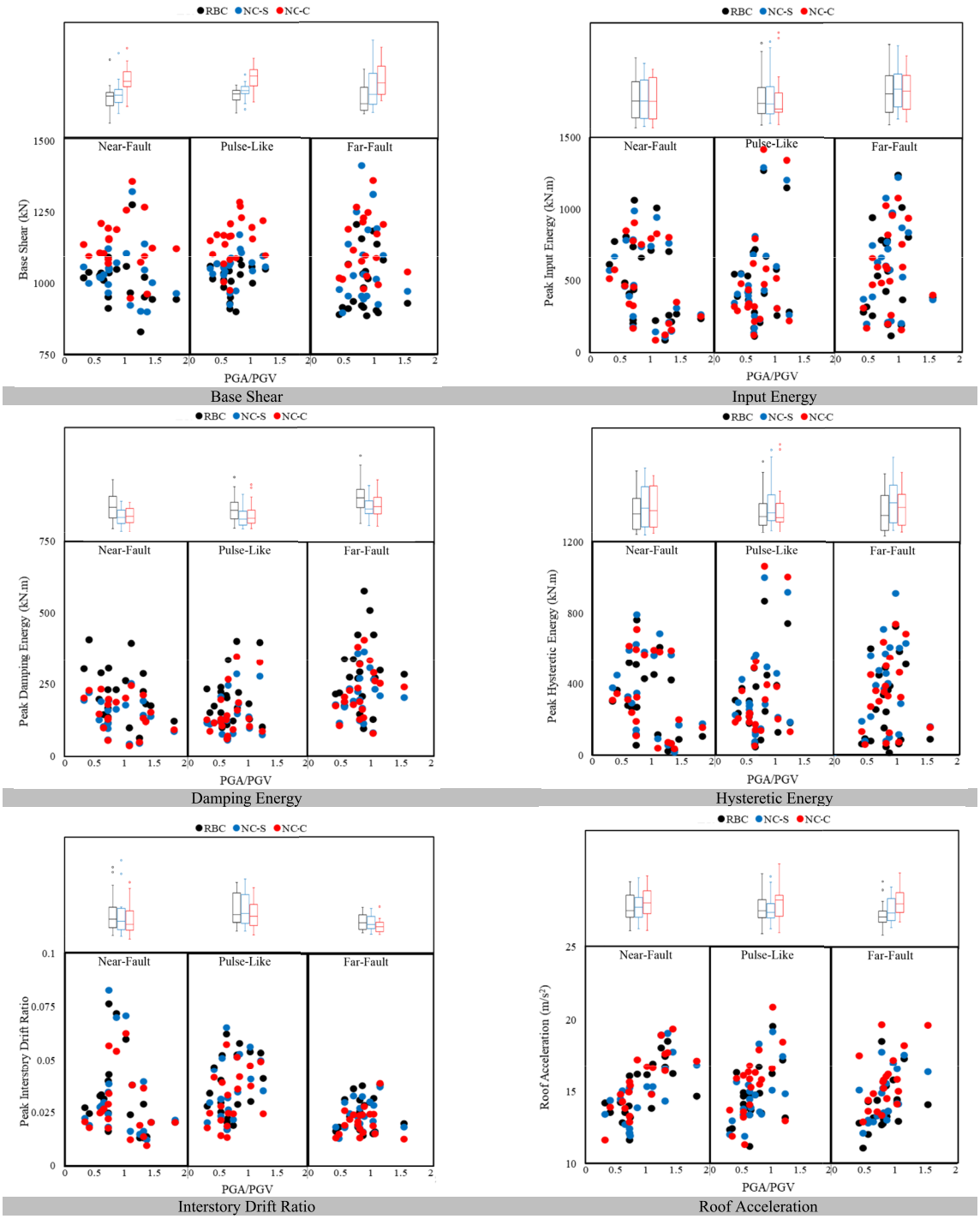

Fig. 18. Influence of earthquake intensity on the seismic behavior of the frame structures.

Moreover, RBC follows behaviors previously reported in literature, suggesting that frames similar to those studied here are more affected by earthquakes with medium PGA/PGV values.

Figure 19, Fig. 20, and Fig. 21 illustrate the seismic behavior of frame structures in the time domain under near-fault, pulse-like, and far-fault earthquakes, respectively. As discussed earlier, the base shear forces and roof accelerations of the RBC frame generally surpassed those of both NC-S and NC-C in all scenarios. Additionally, the story displacements of the RBC typically reached the highest values throughout the records for the given ground motion cases, as clearly depicted in the detailed time history plots in Fig. 19, Fig. 20, and Fig. 21. Furthermore, the base shear-roof displacement responses of the mentioned frames under near-fault (Fig. 19), pulse-like (Fig. 20), and far-fault (Fig. 21) records indicate that RBC's behavior is slightly less pronounced than that of NC-S, while it is significantly more pronounced than that of NC-C. This difference is attributed to the

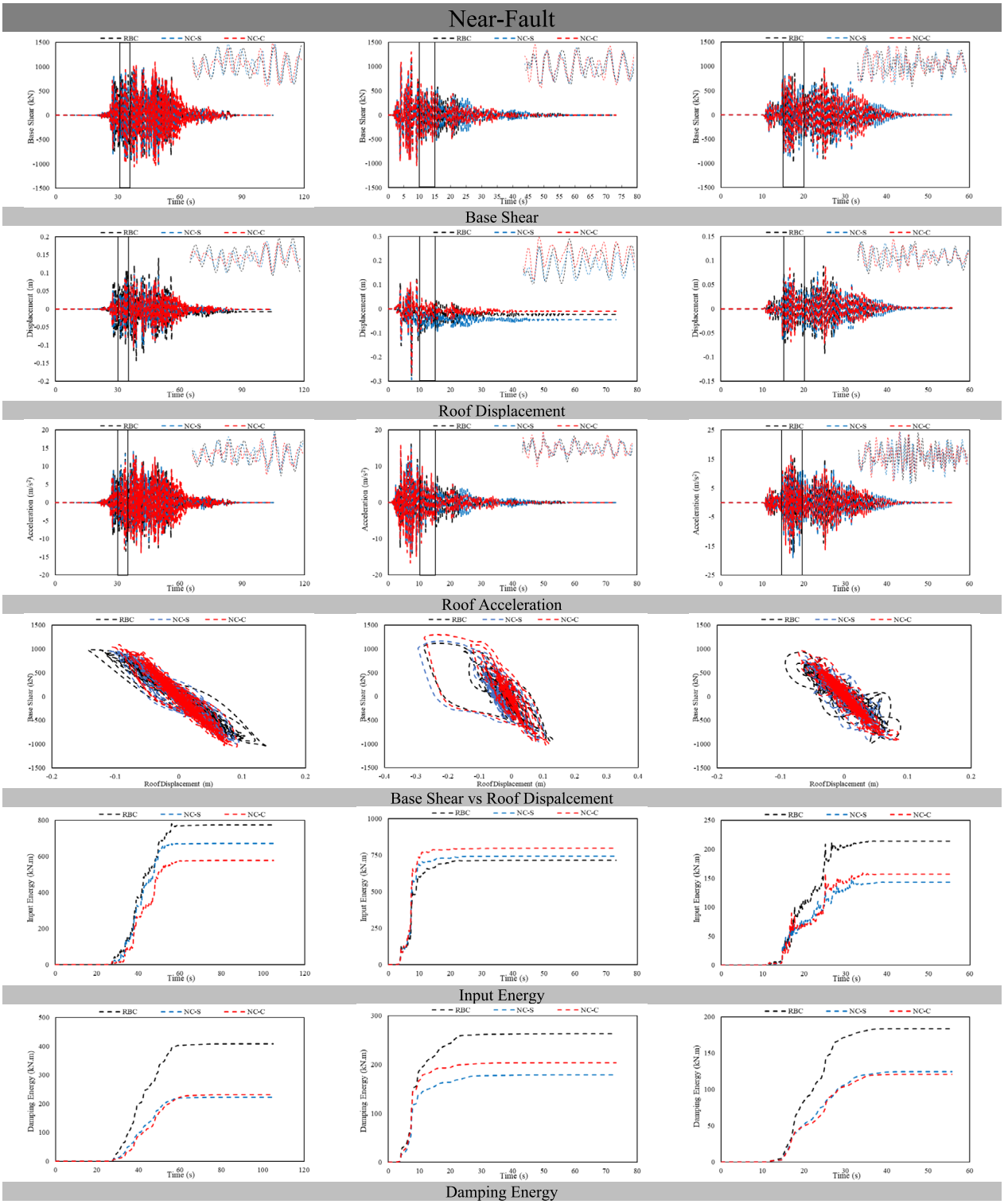

Fig. 19. Seismic behavior of the frame structures under near-fault earthquakes.

variance in their stiffness, which arises from the reduced modulus of elasticity in the RBC mixture. Moreover, the energy distribution in the structures revealed that RBC outperformed other frames in terms of damping energy, while the hysteretic energy showed superior performance in terms of input energy. This suggests that using RBC can result in fewer cracks and less nonlinear degradation of structural elements. Based on these comparisons, several observations are noted:

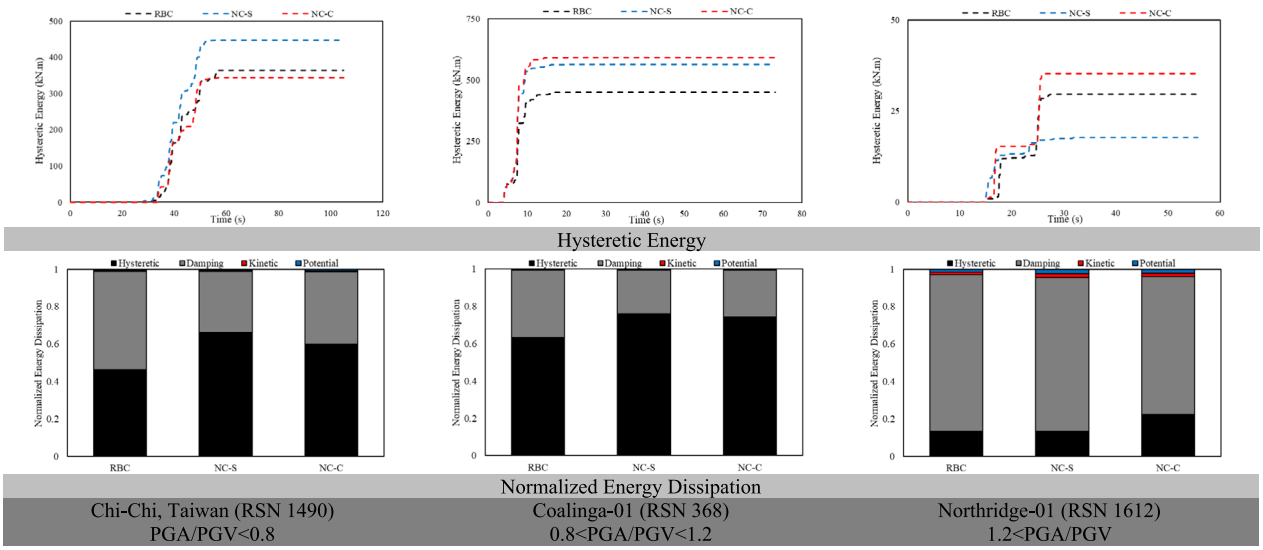

Fig. 19. (continued)

- Despite RBC providing peak base shear force and roof accelerations in certain segments of the time history analysis, particularly in low to medium PGA/PGV ratio cases, its overall behavior was overshadowed by NC-S and NC-C.
- In scenarios involving near-fault and pulse-like ground motions with small to medium PGA/PGV ratios, the RBC frame's displacements peaked more frequently compared to NC-S and NC-C, especially compared to responses observed in far-fault earthquakes.
- Significantly wide hysteresis cycles were reported for pulse-like earthquakes at all PGA/PGV ratios, indicating substantial strength and stiffness degradation and resulting in more cracks. This suggests that pulse-like types exhibit the most severe behavior among others.
- In terms of energy dissipation, RBC demonstrates more efficient behavior under near-fault and far-fault earthquakes compared to pulse-like ones, due to the considerably higher damage that pulse-like ground motions inflict on structures.
- Higher classes of PGA/PGV ratio yield the lowest hysteretic energy, indicating the least damage for the selected low-rise moment-resisting frame structure.

Discussions

The numerical evidence indicates that rubberized concrete can alter the seismic demand pathway in low-rise moment frames in ways that matter for both safety and serviceability. Reduced base shear, averaging up to 11.6–13.8% versus the conventional mix and roughly 3–6% versus the similar-strength mix, translates directly into lower column and foundation actions for the same hazard, which eases shear and flexural design checks and can moderate demands on anchorage, collector forces, and diaphragm chords. From a safety perspective, smaller global forces lessen the probability of brittle shear failures and ease P-Δ amplification, particularly in first-story columns where gravity axial loads are highest. Serviceability benefits follow as well: lower base shear tends to reduce residual force-driven damage to connections and joints, even when peak drifts are comparable. The accompanying drift increase stems from the lower elastic stiffness and extended fundamental period. In the investigated frames, peak interstory drift ratios remained within ASCE 7 limits, which suggests that life-safety objectives are not compromised; however, the drift shift has implications for nonstructural performance. Partition cracking, facade damage, and suspended systems are more sensitive to drift than to inertia alone. Where architectural drift limits govern, designers may need to refine story stiffness distribution, adjust beam-column sizing, or add economical drift-control measures such as strategically placed walls or supplemental dampers with modest coefficients. The observed reduction in absolute floor accelerations, most pronounced for far-fault motions, indicates potential mitigation of acceleration-sensitive components, equipment, and contents, partially offsetting the drift trade-off. Enhanced viscous damping energy and reduced hysteretic energy point to a favorable damage mechanism. Greater viscous participation means a larger share of input energy is dissipated through material damping rather than plastic excursions, which aligns with the time-history evidence of fewer and narrower hysteresis loops in the rubberized frames. Practically, this can delay bar fracture, limit cumulative low-cycle fatigue, and reduce the extent of concrete spalling and residual crack widths after strong shaking. Such behavior supports faster post-event functionality and lower repair scope, a serviceability advantage that complements the safety gains from reduced demand. Design translation is straightforward. Spectral procedures that rely on effective period and damping can be adapted by assigning a higher effective damping ratio, then checking that the increased period does not trigger unacceptable drift. Member design may use similar flexural capacities as a comparable-strength mix, while shear checks and foundation design benefit from the reduced base reactions. Detailing should reflect expected ductility demands at the higher drift plateau, preserving

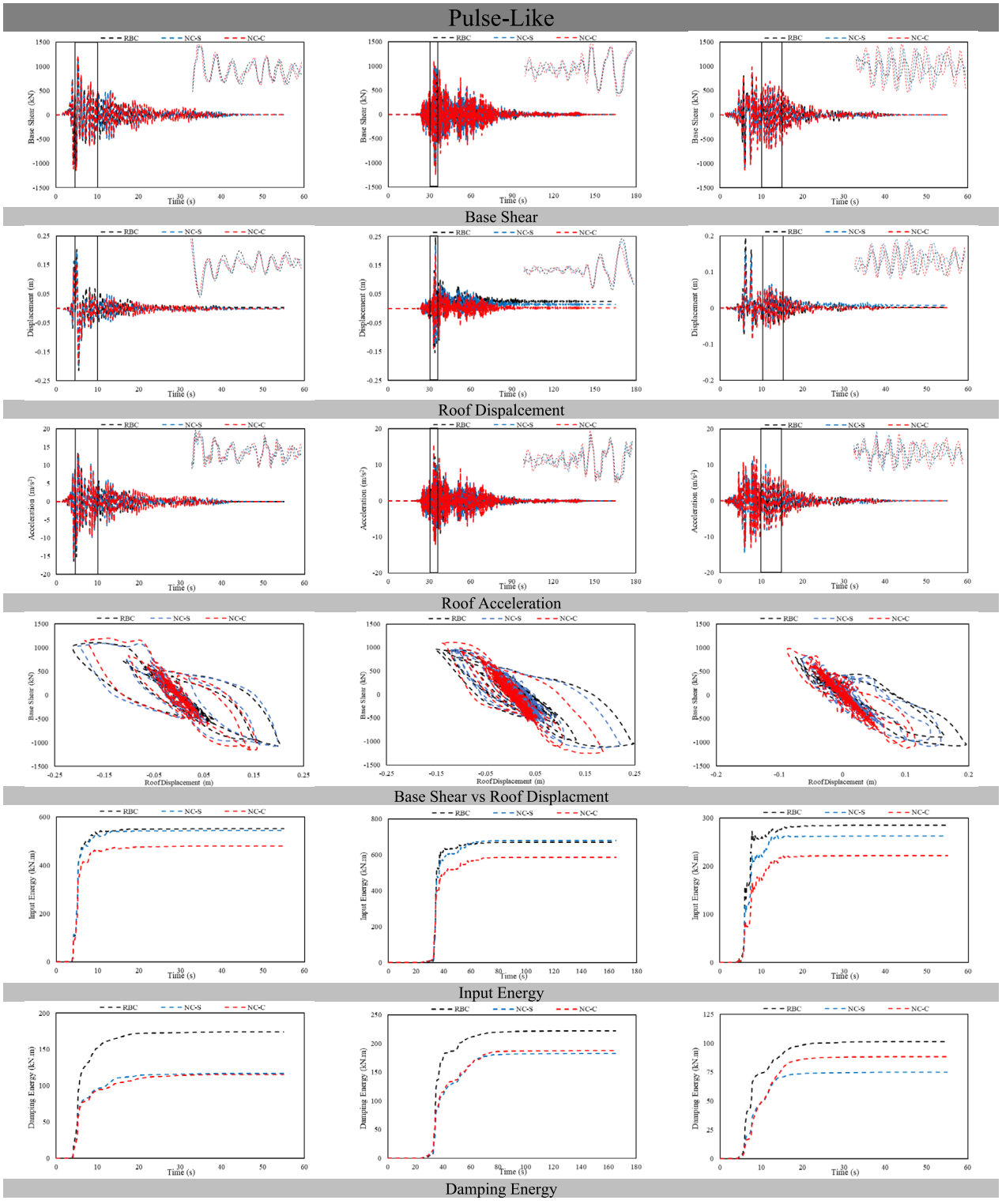

Fig. 20. Seismic behavior of the frame structures under pulse-like earthquakes.

confinement and bar development consistent with modern frame provisions. For retrofit or cost-conscious projects, the material presents a low-intrusion path to improved damping with measurable reductions in force demand, provided serviceability is safeguarded through targeted stiffness tuning and nonstructural drift protection.

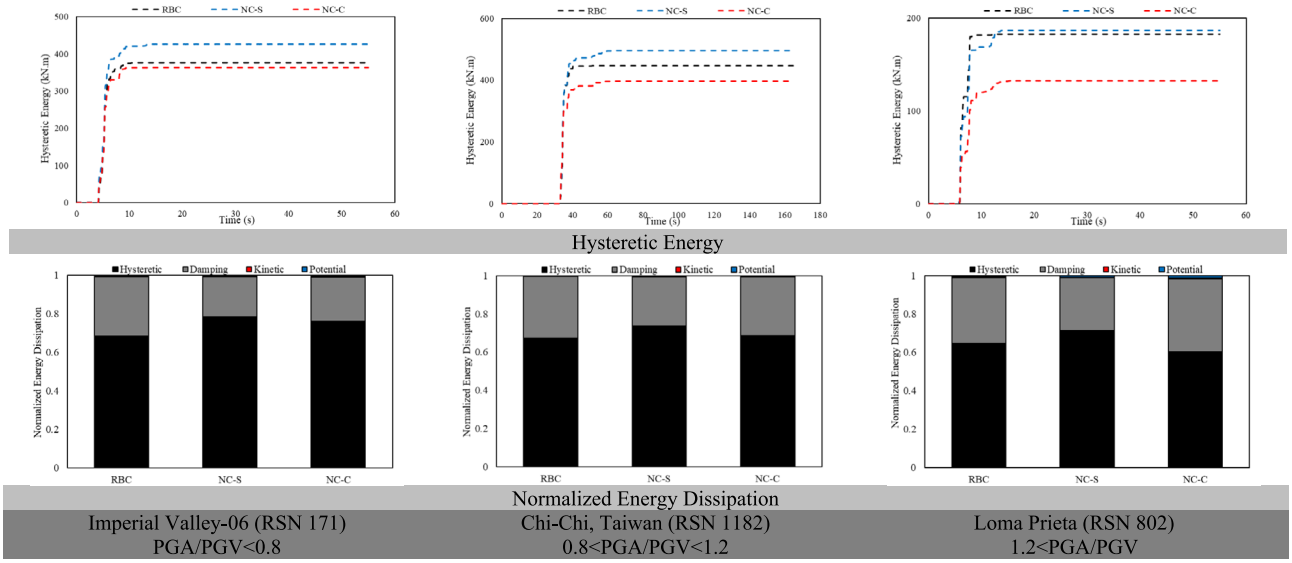

Fig. 20. (continued)

Conclusion

This study, focusing on the seismic behavior and efficiency of RBC in RC low-rise moment-resisting frames, indicates measurable shifts in demand and energy pathways supported by statistics from sixty recorded ground motions. Utilizing RBC in structures decreased mean base shear by 11.6–13.8% compared to NC-C and by approximately 3–6% compared to NC-S, while the fundamental period increased by about 17% versus NC-S and 25.2% versus NC-C. The input energy of the structure was not significantly influenced by the concrete type; however, the energy distribution changed: peak viscous damping energy increased by roughly 29–53% across motion classes, and peak hysteretic energy declined by about 10–29%. The mean interstory drift ratio for RBC generally exceeded that of NC yet stayed within the ASCE 7 drift limit of 4%, and absolute floor accelerations showed modest relief, with up to 11.8% reduction in far-fault earthquakes. The base shear–roof displacement behavior of the RBC frame was substantially lower than the NC-C model and generally comparable to NC-S, indicating that the damping gains are achieved at a manageable drift trade-off. The scope of the analysis imposes limitations that frame these findings. Only low-rise frames on Site Class D were studied with a deliberately weak design; generalization to mid- or high-rise buildings, wall–frame systems, or stiffer archetypes should be made with caution. Soil–structure interaction was neglected through a fixed-base idealization, and inherent damping was represented via Rayleigh coefficients with RBC damping imposed as calibrated ratios rather than micromechanical models. Beam–column joints were not assigned explicit joint-shear springs, bond-slip was not modeled, and records were applied as a single horizontal component using an MSE scaling procedure. Material variability, aging, and environmental effects were not evaluated; the RBC properties reflected a single coarse-rubber replacement level (≈15%). A comprehensive parametric exploration of damping representations and rubber content was not undertaken because mixture-specific viscoelastic calibration data were not available; this limitation is acknowledged and explicitly deferred to future work. Future work can extend these results through targeted parametric, sensitivity, and optimization analyses spanning rubber content ratio, ground-motion intensity measures (including PGA/PGV classes), frame height and system type, and alternative damping assumptions to map efficacy ranges and drift thresholds. Large-scale experimental validation at component and frame levels that captures joint behavior, bond development, and cumulative damage would strengthen confidence in the reported energy trends. Hybrid or graded mixes that recover stiffness while retaining damping, as well as assessments that incorporate SSI, both horizontal components, and nonstructural fragility, repair cost, and downtime, would broaden applicability. Code-oriented developments for assigning effective damping and modified spectra for RBC frames, supported by probabilistic collapse and loss analyses, could translate these findings into practical design guidance.

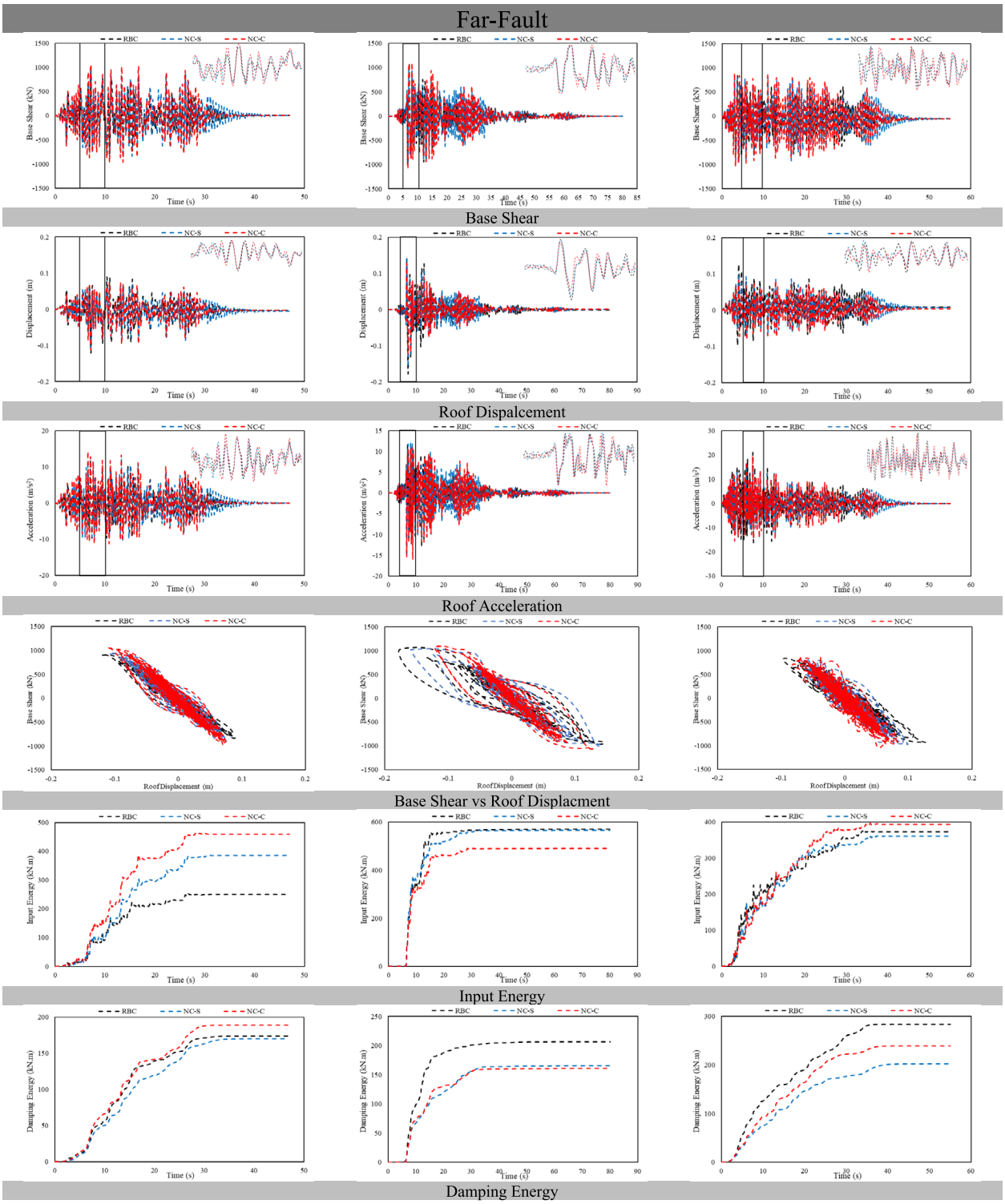

Fig. 21. Seismic behavior of the frame structures under far-fault earthquakes.

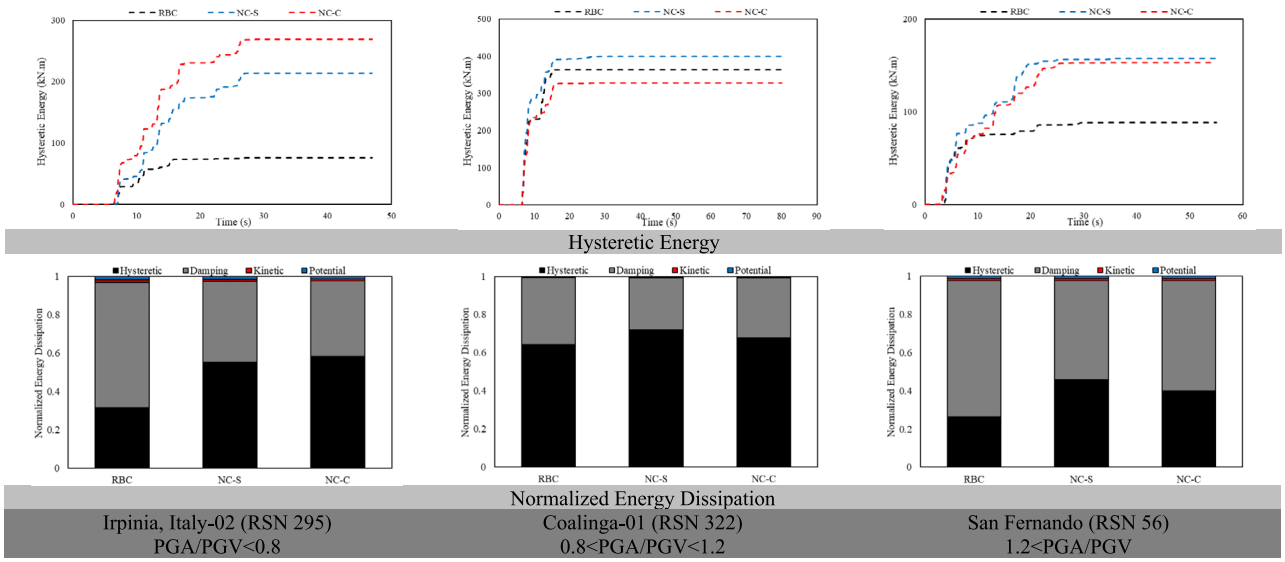

Fig. 21. (continued)

Data availability

The data that support the findings of this study are available from the corresponding author upon reasonable request.

Received: 3 September 2025; Accepted: 29 October 2025
Published online: 27 November 2025

References

1. Dolšek, M. & Fajfar, P. Inelastic spectra for infilled reinforced concrete frames. *Earthquake Eng. Struct. Dynam.* **33**(15), 1395–1416 (2004).
2. Mahmoud, S., Genidy, M. & Tahoon, H. Time-History analysis of reinforced concrete frame buildings with soft storeys. *Arab. J. Sci. Eng.* **42**(3), 1201–1217 (2017).
3. Habib, A., Barakat, S., Al-Toubat, S., Junaid, M. T. & Maalej, M. Developing machine learning models for identifying the failure potential of fire-exposed FRP-strengthened concrete beams. *Arab. J. Sci. Eng.* **50**(11), 8475–8490 (2025).
4. Al Houri, A., Habib, A. & Al-Sadoon, Z. A. Artificial intelligence-based design and analysis of passive control structures: An overview. *J. Soft Comput. Civil Eng.* **9**(3), 137–168 (2025).
5. George, C. & Selvan, S. S. State of Art—Light gauge steel hollow and in-filled columns and beams under elevated temperature. *Iran. J. Sci. Technol., Trans. Civil Eng.* **47**(3), 1265–1276 (2023).
6. George, C. & Selvan, S. S. Integrated analysis of light gauge steel beam sections enhanced by steel fiber reinforced concrete: A comprehensive study on structural and thermal performance. *Matéria (Rio de Janeiro)* **29**(2), e20230329 (2024).
7. Habib, A., Alnaemi, A. & Habib, M. Developing a framework for integrating blockchain technology into earthquake risk mitigation and disaster management strategies of smart cities. *Smart Sustain. Built Environ.* https://doi.org/10.1108/SASBE-12-2023-0376 (2024).
8. Moustafa, A., Gheni, A. & ElGawady, M. A. Shaking-Table testing of high energy-dissipating rubberized concrete columns. *J. Bridg. Eng.* **22**(8), 04017042 (2017).
9. Habib, A. & Yildirim, U. Distribution of strong input energy in base-isolated structures with complex nonlinearity: A parametric assessment. *Multidiscip. Model. Mater. Struct.* **19**(2), 324–340 (2023).
10. George, C. & Senthil Selvan, S. Analyzing the structural and thermal behavior of beam sections filled with steel fiber-reinforced concrete in light-gauge steel. *Adv. Mater. Struct.* **32**(8), 1594–1609 (2025).
11. George, C. et al. Enhancing the fire-resistant performance of concrete-filled steel tube columns with steel fiber-reinforced concrete. *Case Stud. Constr. Mater.* **20**, e02741 (2024).
12. Kitayama, S. & Constantinou, M. C. Seismic performance of buildings with viscous damping systems designed by the procedures of ASCE/SEI 7–16. *J. Struct. Eng.* **144**(6), 04018050 (2018).
13. Seo, C. Y., Karavasilis, T. L., Ricles, J. M. & Sause, R. Seismic performance and probabilistic collapse resistance assessment of steel moment resisting frames with fluid viscous dampers. *Earthquake Eng. Struct. Dynam.* **43**(14), 2135–2154 (2014).
14. Kelly, J. M. Seismic isolation systems for developing countries. *Earthq. Spectra* **18**(3), 385–406 (2002).
15. Hadad, H. A., Calabrese, A., Strano, S. & Serino, G. A base isolation system for developing countries using discarded tyres filled with elastomeric recycled materials. *J. Earthquake Eng.* **21**(2), 246–266 (2017).
16. Dalela, S., Balaji, P. S., Leblouba, M., Trivedi, S. & Kalam, A. Nonlinear static and dynamic response of a metastructure exhibiting quasi-zero-stiffness characteristics for vibration control: An experimental validation. *Sci. Rep.* **14**(1), 19195 (2024).
17. Alam, I., Mahmood, A. & Khattak, N. Use of rubber as aggregate in concrete: A Review. *Int. J. Adv. Struct. Geotech. Eng.* **4**, 92–96 (2015).
18. Li, D. et al. Review of the performance of high-strength rubberized concrete and its potential structural applications. *Adv. Civil Eng. Mater.* **5**, 149–166 (2016).
19. Thomas, B. S. & Gupta, R. C. A comprehensive review on the applications of waste tire rubber in cement concrete. *Renew. Sustain. Energy Rev.* **54**, 1323–1333 (2016).
20. Najim, K. B. & Hall, M. R. A review of the fresh/hardened properties and applications for plain- (PRC) and self-compacting rubberised concrete (SCRC). *Constr. Build. Mater.* **24**, 2043–2051 (2010).

21. Xue, J. & Shinozuka, M. Rubberized concrete: A green structural material with enhanced energy-dissipation capability. *Constr. Build. Mater.* **42**, 196–204 (2013).
22. Gintautas, S., Gintautas, S. & Kęstutis, M. Damping properties of concrete with rubber waste additives. *Mater. Sci. (Medžiagotyra)* **15**(3), 266–272 (2009).
23. Eldin, N. N. & Senouci, A. B. Engineering properties of rubberized concrete. *Can. J. Civil Eng.* **19**, 912–923 (1992).
24. Fattuhi, N. I. & Clark, L. A. Cement-based materials containing shredded scrap truck tyre rubber. *Constr. Build. Mater.* **10**, 229–236 (1996).
25. Khatib, Z. K. & Bayomy, F. M. Rubberized portland cement concrete. *J. Mater. Civil Eng.* **11**, 206–213 (1999).
26. Zheng, L., Huo, X. S. & Yuan, Y. Strength, modulus of elasticity, and brittleness index of rubberized concrete. *J. Mater. Civil Eng.* **20**, 692–699 (2008).
27. Habib, A., Yildirim, U. & Eren, O. Mechanical and dynamic properties of high strength concrete with well graded coarse and fine tire rubber. *Constr. Build. Mater.* **246**, 118502 (2020).
28. Habib, A., Yidirim, U. & Eren, O. Properties of high-strength concrete containing well graded rubber particles. *IOP Conf. Series Mater. Sci. Eng.* **800**, 012018 (2020).
29. Bisht, K. & Ramana, P. V. Evaluation of mechanical and durability properties of crumb rubber concrete. *Constr. Build. Mater.* **155**, 811–817 (2017).
30. Habib, A. & Yildirim, U. Simplified modeling of rubberized concrete properties using multivariable regression analysis. *Mater. Constr.* **72**(347), e289–e289 (2022).
31. Mendis, A. S., Al-Deen, S. & Ashraf, M. Behaviour of similar strength crumbed rubber concrete (CRC) mixes with different mix proportions. *Constr. Build. Mater.* **137**, 354–366 (2017).
32. Youssf, O., ElGawady, M. A. & Mills, J. E. Experimental investigation of crumb rubber concrete columns under seismic loading. *Structures* **3**, 13–27 (2015).
33. Youssf, O., ElGawady, M. A. & Mills, J. E. Static cyclic behaviour of FRP-confined crumb rubber concrete columns. *Eng. Struct.* **113**, 371–387 (2016).
34. ACI. ACI 318–19: Building code requirements for structural concrete and commentary. *Farmington Hills, USA: Am. Concrete Institute* https://doi.org/10.14359/51716937 (2019).
35. -ASCE, ASCE/SEI 7–16 Minimum Design Loads For Buildings and Other Structures. (2016).
36. NIST,. Guidelines for nonlinear structural analysis for design of buildings part IIb – reinforced concrete moment frames. *Nat. Inst. Standards Technol.* https://doi.org/10.6028/NIST.GCR.17-917-46V3 (2017).
37. Mander, J. B., Priestley, M. J. & Park, R. Theoretical stress-strain model for confined concrete. *J. Struct. Eng.* **114**(8), 1804–1826 (1988).
38. Park, R. & Paulay, T. Reinforced concrete structures. *Wiley* https://doi.org/10.1002/9780470172834 (1975).
39. Avşar, Ö., Bayhan, B. & Yakut, A. Effective flexural rigidities for ordinary reinforced concrete columns and beams. *Struct. Design Tall Spec. Build.* **23**(6), 463–482 (2014).
40. Kwon, J. *Strength, Stiffness, and Damage of Reinforced Concrete Buildings, Austin* (University of Texas at Austin, 2016).
41. Kalantari, A. & Roohbakhsh, H. Expected seismic fragility of code-conforming RC moment resisting frames under twin seismic events. *J. Build. Eng.* **28**, 101098 (2020).
42. Michaud, D. & Léger, P. Ground motions selection and scaling for nonlinear dynamic analysis of structures located in Eastern North America. *Can. J. Civ. Eng.* **41**(3), 232–244 (2013).
43. -ATC, ATC-63: Quantification of building seismic performance factors, California: US Department of Homeland Security, FEMA-P695. (2009).
44. -ASCE, ASCE/SEI 7–05: Minimum design loads for buildings and other structures, Virginia: American Society of Civil Engineers. (2005).
45. Mir, F. U. H. & Rai, D. C. Experimental and parametric investigation of effects of built-in staircases on the dynamics of RC buildings. *Earthquake Eng. Struct. Dynam.* **49**(6), 527–542 (2020).
46. -CSI, "SAP2000 - Structural Software for Analysis and Design," Computers and Structures Inc., California.
47. Su, H., Yang, J., Ling, T. C., Ghataora, G. S. & Dirar, S. Properties of concrete prepared with waste tyre rubber particles of uniform and varying sizes. *J. Clean. Prod.* **91**, 288–296 (2015).
48. -FEMA, Hazus-MH MR5 Technical Manual, Washington, D.C. (2010).
49. -A. K. Kazantzi and D. Vamvatsikos, "A study on the correlation between dissipated hysteretic energy and seismic performance," in *World Conference on Earthquake Egineering*, Lisboa. (2015).
50. Zhu, T. J., Heidebrecht, A. C. & Tso, W. K. Effect of peak ground acceleration to velocity ratio on ductility demand of inelastic systems. *Earthquake Eng. Struct. Dynam.* **16**(1), 63–79 (1988).
51. Zhu, T. J., Tso, W. K. & Heidebrecht, A. C. Effect of peak ground a/v ratio on structural damage. *J. Struct. Eng.* **114**(5), 1019–1037 (1988).
52. -A. S. Elnashai and L. D. Sarno, Fundamentals of earthquake engineering. Wiley. (2015).
53. Habib, A. & Yildirim, U. Influence of isolator properties and earthquake characteristics on the seismic behavior of RC structure equipped with quintuple friction pendulum bearings. *Int. J. Struct. Stab. Dyn.* **23**(06), 2350060 (2023).

Author contributions

The authors confirm their contribution to the paper as follows: study conception and design: A. H., M. L., T. J., S. A., M. M., and M. H.; analysis and interpretation of results: A. H., M. L., T. J., S. A., M. M., and M. H.; draft manuscript preparation: A. H., M. L., and T. J.; manuscript review & editing: S. A., M. M., and M. H. All authors reviewed the results and approved the final version of the manuscript.

Funding

This research did not receive any specific grant from funding agencies in the public, commercial, or not-for-profit sectors.

Declarations

Competing interests

The authors declare no competing interests.

Additional information

Correspondence and requests for materials should be addressed to M.H.

Reprints and permissions information is available at www.nature.com/reprints.